


# Scalable fabrication of $Bi_2O_2Se$ polycrystalline thin film for near-infrared optoelectronic devices applications

Bin Liu(刘斌) and Hong Zhou(周洪)

**Citation:**Chin. Phys. B, 2021, 30 (**10**): 106803. DOI: 10.1088/1674-1056/ac1571
Journal homepage: http://cpb.iphy.ac.cn; http://iopscience.iop.org/cpb

**What follows is a list of articles you may be interested in**

---

## Phase transition-induced superstructures of *β*-Sn films with atomic-scale thickness

Le Lei(雷乐), Feiyue Cao(曹飞跃), Shuya Xing(邢淑雅), Haoyu Dong(董皓宇), Jianfeng Guo(郭剑锋), Shangzhi Gu(顾尚志), Yanyan Geng(耿燕燕), Shuo Mi(米烁), Hanxiang Wu(吴翰翔), Fei Pang(庞斐), Rui Xu(许瑞), Wei Ji(季威), and Zhihai Cheng(程志海)
Chin. Phys. B, 2021, 30 (**9**): 096804. DOI: 10.1088/1674-1056/ac11e8

## Probing thermal properties of vanadium dioxide thin films by time-domain thermoreflectance without metal film

Qing-Jian Lu(陆青鑑), Min Gao(高敏), Chang Lu(路畅), Fei Long(龙飞), Tai-Song Pan(潘泰松), and Yuan Lin(林媛)
Chin. Phys. B, 2021, 30 (**9**): 096801. DOI: 10.1088/1674-1056/abea94

## Effect of Mo doping on phase change performance of $Sb_2Te_3$

Wan-Liang Liu(刘万良), Ying Chen(陈莹), Tao Li(李涛), Zhi-Tang Song(宋志棠), and Liang-Cai Wu(吴良才)
Chin. Phys. B, 2021, 30 (**8**): 086801. DOI: 10.1088/1674-1056/abe22d

## PEALD-deposited crystalline GaN films on Si (100) substrates with sharp interfaces

San-Jie Liu(刘三姐), Ying-Feng He(何荧峰), Hui-Yun Wei(卫会云), Peng Qiu(仇鹏), Yi-Meng Song(宋祎萌), Yun-Lai An(安运来), Abdul Rehman(阿布度-拉赫曼), Ming-Zeng Peng(彭铭曾), Xin-He Zheng(郑新和)
Chin. Phys. B, 2019, 28 (**2**): 026801. DOI: 10.1088/1674-1056/28/2/026801

## High quality $PdTe_2$ thin films grown by molecular beam epitaxy

En Li(李恩), Rui-Zi Zhang(张瑞梓), Hang Li(李航), Chen Liu(刘晨), Geng Li(李更), Jia-Ou Wang(王嘉鸥), Tian Qian(钱天), Hong Ding(丁洪), Yu-Yang Zhang(张余洋), Shi-Xuan Du(杜世萱), Xiao Lin(林晓), Hong-Jun Gao(高鸿钧)
Chin. Phys. B, 2018, 27 (**8**): 086804. DOI: 10.1088/1674-1056/27/8/086804

---

# Scalable fabrication of $Bi_2O_2Se$ polycrystalline thin film for near-infrared optoelectronic devices applications*

Bin Liu(刘斌) and Hong Zhou(周洪)†

*School of Physics and Electronics, Hunan University, Changsha* 410082, *China*

(Received 25 April 2021; revised manuscript received 27 June 2021; accepted manuscript online 18 July 2021)

We present a controlled, stepwise formation of layered semiconductor $Bi_2O_2Se$ thin films prepared via the vapour process by annealing topological insulator $Bi_2Se_3$ thin films in low oxygen atmosphere for different reactions. Photodetectors based on $Bi_2O_2Se$ thin film show a responsivity of $1.7\times10^4$ A/W at a wavelength of 980 nm. Field-effect transistors based on $Bi_2O_2Se$ thin film exhibit n-type behavior and present a high electron mobility of 17 $cm^2/V{\cdot}s$. In addition, the electrical properties of the devices after 4 months keeping in the air shows little change, implying outstanding air-stability of our $Bi_2O_2Se$ thin films. From the obtained results, it is evident that low oxygen annealing is a surprisingly effective method to fabricate $Bi_2O_2Se$ thin films for integrated optoelectronic applications.

**Keywords:** thin films, $Bi_2Se_3$, vapor-phase deposition, photodetector, $Bi_2O_2Se$

**PACS:** 68.55.–a, 81.10.Bk, 85.60.Gz **DOI:** 10.1088/1674-1056/ac1571

## 1. Introduction

Two-dimensional (2D) semiconducting layered materials are currently at the forefront of electronic and optoelectronics research because of their numerous desirable properties and are a promising candidate for next-generation integrated circuit technology.[1–5] With only a few years of research, a great number of 2D semiconductors have been isolated or synthesized, including transition metal-dichalcogenides (TMD)[6] and black phosphorus (BP),[7] and other group-VA materials.[8] However, these materials are facing issues towards practical application, such as the need to achieve high carrier mobility, and ambient environment stability.[9–11] $MoS_2$, for example, is a robust TMD material for 2D electronics with tunable bandgap. However, the relatively low carrier mobility ($<$ 200 $cm^2/V{\cdot}s$ at room temperature) hinders its application in high-frequency optoelectronic devices.[12] BP is known for its widely layer-tunable direct band gap ($\sim$ 0.3 eV to $\sim$ 2.0 eV) and relatively high carrier mobility ($\sim$ 1000 $cm^2/V{\cdot}s$ at room temperature).[7] However, the degradation of BP under ambient conditions causes functional failure of devices. Since the electrical performance and stability in the ambient environment are key properties for practical applications, it is necessary to search new, stable 2D semiconductors with superior electronic properties.

Recently, layered bismuth oxyselenide ($Bi_2O_2Se$) has been rediscovered as an attractive 2D semiconductor for various applications in electronics and optoelectronics due to its remarkable stability, ultrahigh carrier mobility, and ultrafast broadband photoresponse.[13–17] In addition, $Bi_2O_2Se$ is also promising for ferroelectric and thermoelectric applications.[18–21] At present, chemical vapor deposition (CVD) is the most widely employed technique for the fabrication of $Bi_2O_2Se$, including nanoplates and thin films.[22,23] In most of these reports, randomly distributed $Bi_2O_2Se$ domains are synthesized on mica substrate and single-crystal $Bi_2O_2Se$ thin films can be grown on lattice-matched substrates.[24] However, the availability of substrates for large-scale $Bi_2O_2Se$ growth by CVD has limited its various applications.

In order to avoid this, it is necessary to develop new synthesis methods which could produce large-scale, high-quality $Bi_2O_2Se$ thin films on diverse substrates, especially on $SiO_2/Si$ substrate. In this paper, we present a facile strategy to fabricate large-scale $Bi_2O_2Se$ thin films by directly conversion of $Bi_2Se_3$ films in a tube furnace where the oxygen content was controlled. If the $Bi_2Se_3$ films are directly exposed to air at high temperature, we can only obtain $Bi_2O_3$ film (see supplementary information: Fig. S1). We attempted to control the oxidation process of $Bi_2Se_3$ films by gradually decrease the oxygen content to form $Bi_2O_2Se$ films. Our annealing growth approach ensures the synthesis of $Bi_2O_2Se$ films on diverse substrates. The photoresponse of these $Bi_2O_2Se$ thin films are comparable to that of the CVD-grown nanoplate counterparts, with responsivity of $1.7\times10^4$ A/W and response time of 30 ms. The direct conversion of $Bi_2Se_3$ thin film to $Bi_2O_2Se$ thin film at low oxygen concentration on various substrates is a crucial first step towards solving the necessary for scalable and facile synthesis challenge for $Bi_2O_2Se$-based integrated electronic and optoelectronic devices.

*Project supported by the Hunan Provincial Natural Science Foundation of China (Grant No. 2019JJ40032).

†Corresponding author. E-mail: zhouhong@hnu.edu.cn

© 2021 Chinese Physical Society and IOP Publishing Ltd 

## 2. Experimental details

### 2.1. Synthesis of $Bi_2Se_3$ thin films

A ceramic boat containing 0.2-mg $Bi_2Se_3$ (99.99%, Alfa Aesar) was placed in the center of a horizontal tube furnace equipped with a quartz tube (1 inch, 1 inch = 2.54 cm in diameter). The substrates were placed 20-cm downstream from the source powder. The entire system was pumped down to 200 mTorr (1 Torr = $1.33322\times10^2$ Pa) using a mechanical pump and then flushed with high-purity argon (Ar 99.999%) and the pressure adjusted to 4 Torr. The Ar flow is then adjusted to 90 sccm. After that, the furnace was heated to 580 °C in 18 min for the growth of $Bi_2Se_3$ thin films and maintained at the growth temperature for 20 min. After the synthetic procedure, the furnace was cooled down slowly to room temperature and maintained with gas flow.

### 2.2. Conversion of $Bi_2Se_3$ to $Bi_2O_2Se$

The conversion process was performed under controlled atmosphere in a home-built CVD system at atmospheric pressure. The as-synthesized $Bi_2Se_3$ thin films were placed in the middle of the tube furnace and annealed under low oxygen concentration atmosphere during different periods of time. To control the oxygen concentration inside the system, the furnace tube was first filled with ambient air. Then, high-purity Ar flow was introduced into the furnace at a flow rate of 20 sccm to gradually decrease the oxygen concentration inside the system. After the annealing procedure finished, the quartz tube furnace was switched off. When the furnace reached room temperature, the Ar flow was switched off and the sample was removed.

### 2.3. Material characterizations

Raman spectra were obtained by using a confocal microscope (Invia-reflex, Renishaw, UK) excited at 633-nm laser. The structure of the films was studied using an x-ray diffractometer (XRD-6100, Shimadzu, Japan). A scanning electron microscopy (SEM) (JSM-6700F, Japan) was used to characterize the uniformity of the morphology and distribution of the sample before and after conversion. Chemical information of the sample is obtained by XPS (AXIS SUPRA, Shimadzu, UK) testing. The optical properties of sample were measured by UV-Vis-NIR spectrophotometer (UV-3600 PLUS, Shimadzu).

### 2.4. Device fabrication and electrical and optoelectronic properties characterization

The drain and source electrodes of devices were defined by copper grids shadow mask. Subsequently, Cr/Au (10 nm/50 nm) was deposited by thermal evaporation. The back-gated FETs were fabricated on 300-nm thick $SiO_2$/Si substrates, with $SiO_2$ as dielectrics and $p^{++}$ Si as gate electrode. The electrical and optoelectronic measurement were carried out with a probe station and an Agilent B2902A source meter under ambient conditions at room temperature. The photoresponse was tested using laser diodes at 520 nm, 650 nm, 780 nm, and 980 nm as incident light. The time-resolved photoresponse was measured using a Tektronix TDS2024C oscilloscope.

## 3. Results and discussion

The synthetic route for $Bi_2O_2Se$ thin films involves two steps (Fig. 1(a)). $Bi_2Se_3$ thin films grown by physical vapor deposition (PVD) approach were used as starting materials for the conversion to $Bi_2O_2Se$. The as-grown $Bi_2Se_3$ thin films were then annealed in a low oxygen atmosphere at 400 °C during different periods of time (see Methods section for details). The formation of $Bi_2O_2Se$ was followed using x-ray diffraction (XRD), as shown in Fig. 1(b). The $Bi_2Se_3$ thin film shows a main peak at 18.56° ($2\theta$), which is characteristic of the $Bi_2Se_3$ (006) rhombohedral crystal structure.[25] Notably, only (00l) diffraction peaks are observed in the XRD pattern, indicating that the as-grown $Bi_2Se_3$ film possesses *c*-axis preferential orientation. After 2-h heat treatment there is clear evidence of the formation of $Bi_2O_2Se$ from the appearance of XRD peaks at $2\theta$: 14.80 (002), 29.54 (004), 44.82 (006), representing the formation of tetragonal $Bi_2O_2Se$ crystals. After 3 hours, the entire $Bi_2Se_3$ film is converted to $Bi_2O_2Se$. Transmission electron microscopy (TEM) was further performed to clarify the crystal structure and crystallinity of the as-prepared $Bi_2O_2Se$ film. Figure S2(a) shows a low-magnification TEM image of the $Bi_2O_2Se$ film. Corresponding high-resolution TEM image is shown in Fig. S2(b). It can be clearly seen that the film presents crystalline grains with different orientations. the lattice spacings of 6.0 Å, 3.7 Å, and 2.8 Å corresponding to the (001), (101), and (110) planes of tetragonal $Bi_2O_2Se$. The XRD results and the TEM results confirm the presence of polycrystalline $Bi_2O_2Se$ films. In a recent study, $Bi_2SeO_5$ was obtained by treating $Bi_2O_2Se$ under an oxidation temperature of 370 °C–400 °C in air.[26] In our study, further increase in the annealing time beyond 3 hours did not lead to form $Bi_2SeO_5$ phase (see Supplementary-information, Fig. S3), which indicates the oxygen concentration in the furnace is relatively low. Scanning electron microscopy (SEM) was used to study the surface morphology of the $Bi_2Se_3$ thin films before and after annealing. The as-prepared $Bi_2Se_3$ thin films have a very smooth surface morphology and appear to be quite dense (Fig. 1(c)). After 3-h annealing, significant morphological changes are observed (Fig. 1(d)). Small crystals grow bigger $Bi_2O_2Se$ crystals. Significant advantages of this growth method include simplicity and scalability. In particular, the method can be applicable to a range of substrates that can withstand process temperatures of roughly up to 400 °C, making it practically applicable in diverse fields. As examples of substrate independence, we have successfully fabricated $Bi_2O_2Se$ thin films on ITO, mica and sapphire substrates (see supplementary-information, Fig. S4). A clear change in color is observed from brown to light brown, which indicates the complete conversion of $Bi_2Se_3$ into $Bi_2O_2Se$.

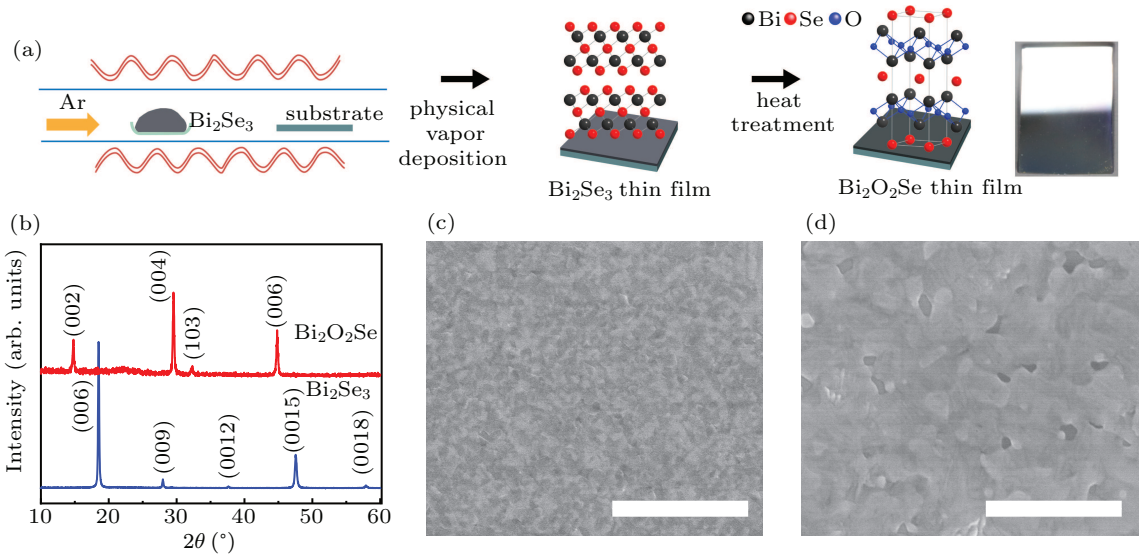



**Fig. 1.** Fabrication of $Bi_2O_2Se$ thin films on $SiO_2$/Si substrates. (a) Schematic illustration of the fabrication process of $Bi_2O_2Se$ thin films using a two-step approach. $Bi_2Se_3$ films are deposited using physical vapor deposition technique at 580 °C for 20 min. Then the films are heated at 400 °C for 3 hours at lower oxygen concentration. The photograph shows the fabricated $Bi_2O_2Se$ film had a mirror-like reflection, indicating high uniformity. (b) Evolution of the XRD patterns as a function of the heat treatment time of the $Bi_2Se_3$ film in a low oxygen atmosphere, showing the transformation of phase from rhombohedral structure ($Bi_2Se_3$) to tetragonal structure ($Bi_2O_2Se$). Top view SEM images of the as-deposited $Bi_2Se_3$ film before (c) and after (d) annealing. Scale bar, 2 μm.

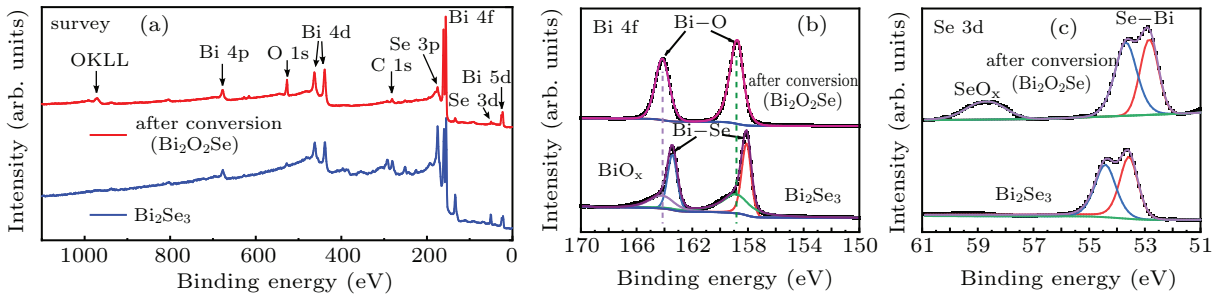



**Fig. 2.** XPS spectra of $Bi_2Se_3$ thin film and $Bi_2O_2Se$ thin film: (a) survey scans, (b) Bi 4f, and (c) Se 3d.

To get further insights into the low oxygen annealing reaction, the x-ray photoelectron spectroscopy (XPS) was carried out on the $Bi_2Se_3$ thin film deposited on $SiO_2$/Si substrates as well as after reaction for 3 hours under low concentration oxygen. The survey scans of these samples are presented in Fig. 2(a) and the characteristic core level peak of $Bi_2Se_3$ and $Bi_2O_2Se$ materials (Bi, O, and Se) are clearly seen. The appearance of a stronger O 1s peak in $Bi_2O_2Se$ while very weak in $Bi_2Se_3$ verifies the successful incorporation of O. Further information on the transition from $Bi_2Se_3$ to $Bi_2O_2Se$ is analyzed via the bonding state and the elemental composition of bismuth (Bi) and selenide (Se), which is obtained looking at the Bi 4f and Se 3d core level peaks presented in Figs. 2(b) and 2(c), respectively. The Bi 4f high-resolution spectrum (Fig. 2(b)) shows two main peaks at binding energy (BE) 163.2 eV and 158.7 eV which could be attributed to Bi–Se bonding in $Bi_2Se_3$, while those at BE 164.2 eV and 158.9 eV are assigned to Bi–O bonding in $Bi_2O_2Se$, respectively.[27] For as-grown $Bi_2Se_3$ thin films, a bismuth oxide ($BiO_x$) peak is observed, which may exist in the hydroxide form.[28] Correspondingly, the BE of Se 3d peaks have a red shift of about 0.7 eV after annealing for 3 hours (Fig. 2(c)), which may result from the electron sharing between $Bi^{3+}$ and $O^{2-}$ because the $Se^{2-}$ bond only with $Bi^{3+}$ in the $Bi_2Se_3$, further indicating the formation of $Bi_2O_2Se$. Meanwhile, selenium oxide ($SeO_x$) is also observed after conversion, which indicates the product of the conversion include $SeO_x$.

The conversion of $Bi_2Se_3$ to $Bi_2O_2Se$ was also investigated using Raman spectroscopy. Some distinct differences were observed between the two types of samples and the relative motion of the various atoms for these observed phonons is presented in Fig. 3(a). For pristine $Bi_2Se_3$ thin film, two peaks located at 131 $cm^{-1}$ and 174 $cm^{-1}$ are seen, which according to Irfan *et al.* are characteristic of the $Bi_2Se_3$ crystal.[29] The first peak refers to the $E_g^2$ mode and the second one refers to the $A_{1g}^2$ mode.[30] Noticeably, the Raman spectrum for the $Bi_2Se_3$ after 3-h reaction time shows only one peak located at 158 $cm^{-1}$, corresponding to the vibration mode $A_{1g}$ of $Bi_2O_2Se$. Raman scattering revealing that $Bi_2Se_3$ thin film has fully converted to $Bi_2O_2Se$ thin film after 3-h annealing in the low oxygen concentration. The optical band gap of the as-prepared $Bi_2O_2Se$ thin film was determined using UV-vis-NIR

absorbance spectroscopy (Fig. 3(b)). The absorbance spectra of $Bi_2O_2Se$ thin film have a broad profile and extends to NIR range. The optical band gap of $Bi_2O_2Se$ thin film is estimated to be 0.85 eV from the corresponding Tauc plot, and the electronic transition is indirect in nature. The band gap energy is slightly higher in energy compared with single crystalline $Bi_2O_2Se$ nanosheet.

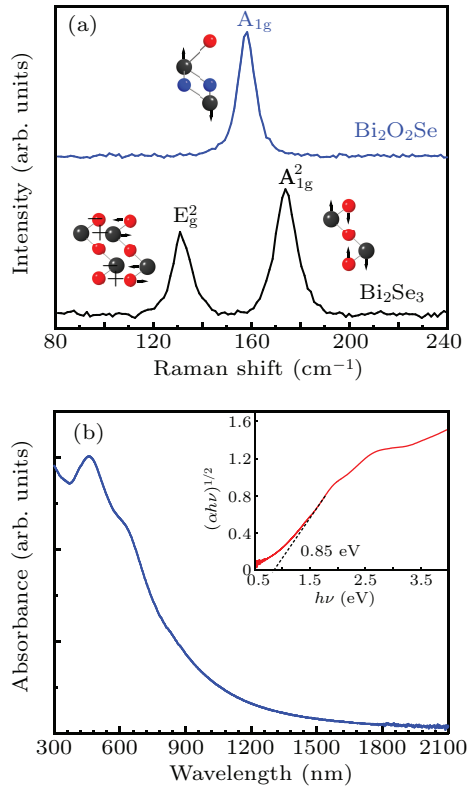



**Fig. 3.** (a) Raman spectra of as-prepared $Bi_2O_2Se$ thin film and pristine $Bi_2Se_3$ thin film. (b) UV-vis-NIR absorption spectra of as-prepared $Bi_2O_2Se$ thin film on fused silica substrate. Inset: Tauc plot corresponds to the indirect optical band gaps of 0.85 eV.

To further explore the optoelectronics applications of $Bi_2O_2Se$ film, the $Bi_2O_2Se$ photodetectors were fabricated directly on $SiO_2$/Si (Fig. 4(a)). Based on large-scale continuous $Bi_2O_2Se$ thin film, photodetectors arrays were then fabricated. The static resistance measurements of 20 devices indicate the good uniformity of our $Bi_2O_2Se$ thin film (see supplementary information, Fig. S5). The current *versus* voltage bias ($I$–$V$) curves of the as-fabricated $Bi_2O_2Se$ photodetector in the dark and in the presence of 980-nm lasers with various power densities at room temperature (Fig. 4(b)). The near linear $I$–$V$ curves indicate an ohmic contact between the $Bi_2O_2Se$ film and the Cr/Au electrodes. Notably, the $Bi_2O_2Se$ films feature excellent environmental stability, with no apparent change in electrical property after months of exposure in air (see supplementary information, Fig. S6). Furthermore, it can be observed that the $Bi_2Se_2O$ device exhibits a prominent sensitivity to near-infrared light and the photocurrent improves obviously with the light intensity increasing. The responsivity ($R$) and detectivity ($D^*$) were calculated to evaluate the photodetection performance of $Bi_2O_2Se$-based photodetectors through the following equations:

$$R = I_{ph}/PS, \tag{1}$$

$$D^* = S^{1/2}R/(2qI_{dark})^{1/2}, \tag{2}$$

where $I_{ph}$ is defined as the photocurrent subtracted by the dark current, $P$ is the incident light intensity, $S$ is the effective illuminated area, $D^*$ only considers the $I_{dark}$ as the major source of shot noise, $q$ is the electronic charge. The light intensity-dependent responsivities at 5-V bias, which reveal that such a photodetector owns a max $R$ and $D^*$, were calculated to be $1.7\times10^4$ A/W and $3.9\times10^{12}$ Jones (1 Jones = 1 cm·$Hz^{1/2}$·$W^{-1}$) under 980-nm light at a low light intensity of 0.001 mW/$cm^2$ (Fig. 4(c)). The $R$ value of the $Bi_2O_2Se$ film is slightly smaller than that of their single crystal counterparts previously reported.[31,32] Besides, figure 4(c) demonstrates that the responsivity of the device decreases with the increase of incident power densities, which is due to enhanced scattering or recombination rate of hot carriers as their density increases at higher laser power.[33]

We next studied the response speed of $Bi_2O_2Se$ film photodetector. Time-dependent photocurrents of the device is displayed in Fig. 4(d), which are operated by periodically turning on and off 980-nm light at a bias of 5.0 V. It can be seen that our device exhibits excellent repeatability, which is suitable for long-term, reliable, and highly sensitive NIR detection/monitoring. A complete on/off cycle in which the photocurrent reveals a fast rise/fall state (Fig. 4(e)). The response time ($\tau_{rise}$) and decay time ($\tau_{fall}$) of the device are estimated to be $\sim$ 89 ms and $\sim$ 30 ms, respectively. The fast response feature is emanated from the high crystalline quality of $Bi_2O_2Se$ film we obtained. The electrical photoresponse variation of the $Bi_2O_2Se$ photodetector for varying incident wavelengths at 5-V bias (Fig. 4(f)). Qualitatively, the photoresponse has a similar wavelength dependence, indicating the realization of a wavelength selective photodetection.

To investigate the electrical transport characteristics of the $Bi_2O_2Se$ film, back-gate FETs were fabricated. As shown in Fig. 5(a), it can be seen from the output characteristic curves of different back-gate voltages that the source–drain current $I_{ds}$ varies linearly with the bias $V_{ds}$ in the range of 0 V–2 V, indicating that a good ohmic contact is formed between the metal electrode and $Bi_2O_2Se$ film. Figure 5(b) shows the transfer curves of the $Bi_2O_2Se$ film at various bias voltage of 0.5 V–3 V, which indicate typical n-type behavior. The calculated average carrier mobilities of the sample is 17 $cm^2$/V·s, which is lower than that of the single-crystalline $Bi_2O_2Se$.[24,34] With $V_{ds}$ increasing from 0.5 V to 3 V, the on-state current can be improved from $2.6\times10^{-5}$ A to $1.8\times10^{-4}$ A. The maximum current on/off ratio ($I_{on}/I_{off}$) is nearly three orders of magnitude, which is lower than that of recently reported single crystalline $Bi_2O_2Se$ nanoplate transistors.[31,35] Furthermore, the

subthreshold swing is deduced to be 1230 mV/dec. The relatively lower carrier mobility and current on/off ratio are likely limited by the structural defect, such as the grain boundary observed by TEM. The annealing conditions of $Bi_2Se_3$ films needs to be studied further for improvement of $Bi_2O_2Se$ films with better crystallographic quality.

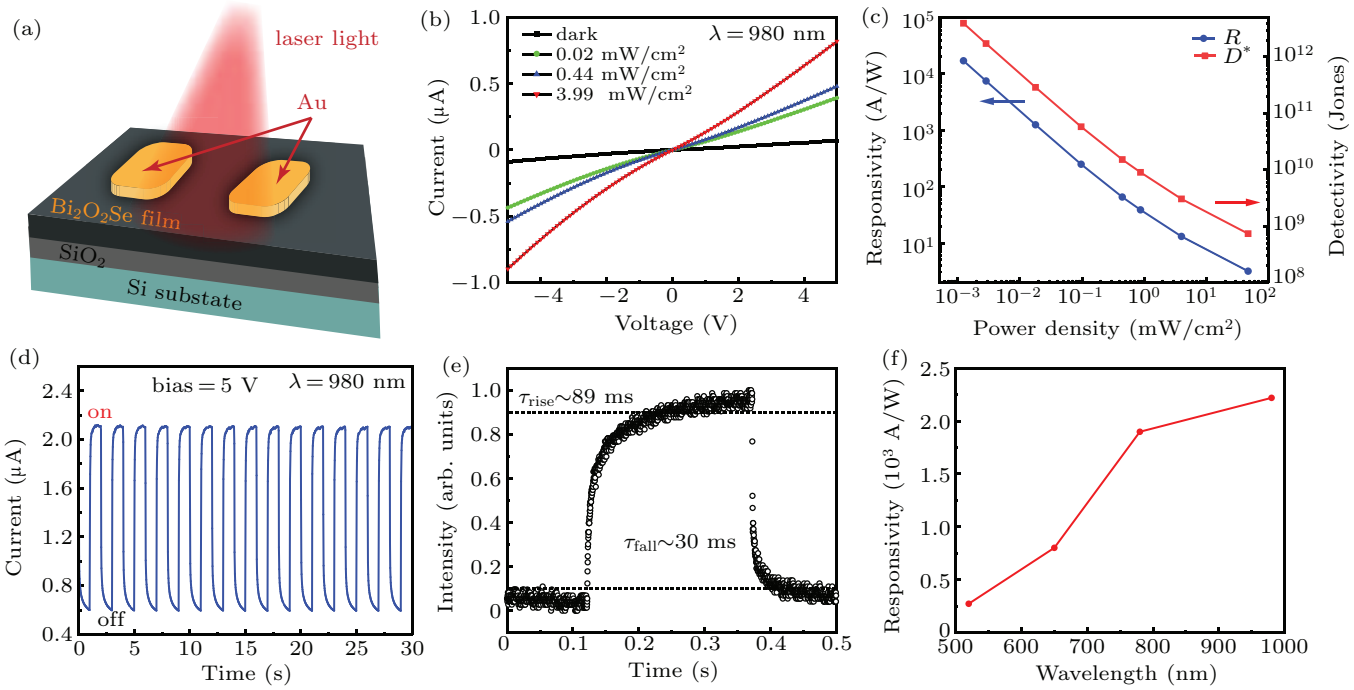



**Fig. 4.** (a) A schematic diagram of the $Bi_2O_2Se$ thin film photodetector on a $SiO_2$/Si substrate. (b) *I*–*V* curves of the $Bi_2O_2Se$ photodetector as a function of light intensity ranging from 0.02 mW/cm$^2$ to 3.99 mW/cm$^2$ (at 980 nm). (c) The plot of photoresponsivity detectivity and $D^*$ *versus* illumination light intensity at 5 V. (d) Reproducible on/off switching illuminated by 980-nm light at a bias of 5 V. (e) Transient response under the illumination of a 980-nm light. (f) The wavelength-dependent photoresponse of the $Bi_2O_2Se$ photodetector at 5-V bias.

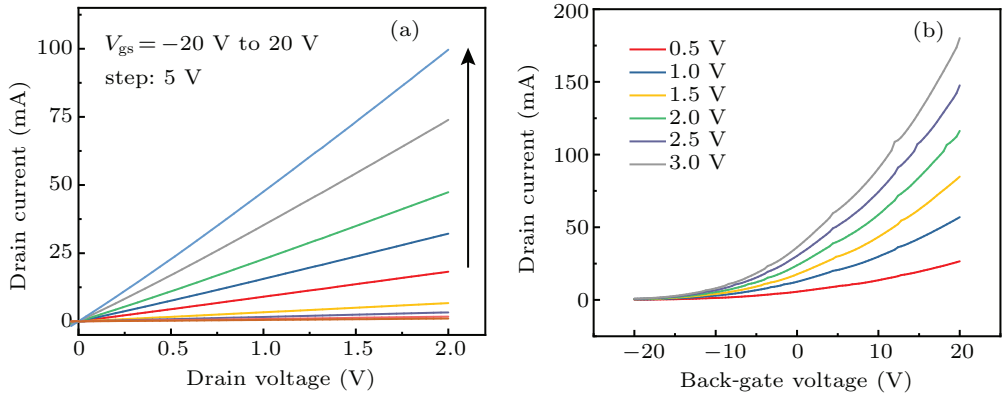



**Fig. 5.** (a) Output characteristics and (b) transfer characteristics of a back-gated $Bi_2O_2Se$ thin film FET measured at room-temperature.

## 4. Conclusion

In summary, we reported a new approach to grow large-area 2D semiconducting $Bi_2O_2Se$ thin films on a wide range of substrates. The prepared $Bi_2O_2Se$ devices exhibited excellent air stability and comparable quality to single-crystalline $Bi_2O_2Se$ with responsivity of $1.7\times10^4$ A/W and response time of 30 ms. All these results reveal that the developed synthesis method can be applied to directly grow $Bi_2O_2Se$ on other high-$\kappa$ dielectrics and opens up the possibility of on-chip fabrication of high-mobility optoelectronic devices with $Bi_2O_2Se$.

## References

[1] Li J, Wang J, Ma J, Shen H, Li L, Duan X and Li D 2019 *Nat. Commun.* **10** 806
[2] Liu J, Zan W, Li K, Yang Y, Bu F and Xu Y 2017 *J. Am. Chem. Soc.* **139** 11666
[3] Hong Y L, Liu Z, Wang L, Zhou T, Ma W, Xu C, Feng S, Chen L, Chen M L, Sun D M, Chen X Q, Cheng H M and Ren W 2020 *Science* **369** 670
[4] Liu C, Chen H, Wang S, Liu Q, Jiang Y G, Zhang D W, Liu M and Zhou P 2020 *Nat. Nanotechnol.* **15** 545
[5] Migliato Marega G, Zhao Y, Avsar A, Wang Z, Tripathi M, Radenovic A and Kis A 2020 *Nature* **587** 72
[6] Wang Q H, Kalantar Zadeh K, Kis A, Coleman J N and Strano M S 2012 *Nat. Nanotechnol.* **7** 699
[7] Li L, Yu Y, Ye G J, Ge Q, Ou X, Wu H, Feng D, Chen X H and Zhang Y 2014 *Nat. Nanotechnol.* **9** 372

[8] Ding Y, Zhou N, Gan L, Yan X, Wu R, Abidi I H, Waleed A, Pan J, Ou X, Zhang Q, Zhuang M, Wang P, Pan X, Fan Z, Zhai T and Luo Z 2018 *Nano Energy* **49** 200

[9] Tan L, Liu Q, Ding Y, Lin X, Hu W, Cai M Q and Zhou H 2020 *Nano Res.* **13** 557

[10] Lanza M, Smets Q, Huyghebaert C and Li L J 2020 *Nat. Commun.* **11** 5689

[11] Yu Z, Ong Z Y, Li S, Xu J B, Zhang G, Zhang Y W, Shi Y and Wang X 2017 *Adv. Funct. Mater.* **27** 1604093

[12] Cheng L, Zhang C and Liu Y 2020 *Phys. Rev. Lett.* **125** 177701

[13] Tong T, Li W, Qin S, Yuan X, Chen Y, Zhang C, Liu W, Wang P, Hu W, Wang F, Zhang J, Zhang R and Xu Y 2020 *IEEE Electron Dev. Lett.* **41** 1464

[14] Wu J, Liu Y, Tan Z, Tan C, Yin J, Li T, Tu T and Peng H 2017 *Adv. Mater.* **29** 1704060

[15] Li P, Han A, Zhang C, He X, Zhang J, Zheng D, Cheng L, Li L J, Miao G X and Zhang X X 2020 *ACS Nano* **14** 11319

[16] Chen C, Wang M, Wu J, *et al.* 2018 *Sci. Adv.* **4** eaat8355

[17] Wu J, Yuan H, Meng M, Chen C, Sun Y, Chen Z, Dang W, Tan C, Liu Y, Yin J, Zhou Y, Huang S, Xu H Q, Cui Y, Hwang H Y, Liu Z, Chen Y, Yan B and Peng H 2017 *Nat. Nanotechnol.* **12** 530

[18] Ghosh T, Samanta M, Vasdev A, Dolui K, Ghatak J, Das T, Sheet G and Biswas K 2019 *Nano Lett.* **19** 5703

[19] Tan X, Lan J l, Ren G, Liu Y, Lin Y H and Nan C W 2017 *J. Am. Ceram. Soc.* **100** 1494

[20] Yang F, Wang R, Zhao W, Jiang J, Wei X, Zheng T, Yang Y, Wang X, Lu J and Ni Z 2019 *Appl. Phys. Lett.* **115** 193103

[21] Wu M and Zeng X C 2017 *Nano Lett.* **17** 6309

[22] Chen W, Khan U, Feng S, Ding B, Xu X and Liu B 2020 *Adv. Funct. Mater.* **30** 2004960

[23] Hong C, Tao Y, Nie A, Zhang M, Wang N, Li R, Huang J, Huang Y, Ren X, Cheng Y and Liu X 2020 *ACS Nano* **14** 16803

[24] Tan C, Tang M, Wu J, Liu Y, Li T, Liang Y, Deng B, Tan Z, Tu T, Zhang Y, Liu C, Chen J H, Wang Y and Peng H 2019 *Nano Lett.* **19** 2148

[25] Zhang H, Zhang X, Liu C, Lee S T and Jie J 2016 *ACS Nano* **10** 5113

[26] Chowdhury T, Kim J, Sadler E C, Li C, Lee S W, Jo K, Xu W, Gracias D H, Drichko N V, Jariwala D, Brintlinger T H, Mueller T, Park H G and Kempa T J 2020 *Nat. Nanotechnol.* **15** 29

[27] Tu T, Zhang Y, Li T, Yu J, Liu L, Wu J, Tan C, Tang J, Liang Y, Zhang C, Dai Y, Han Y, Lai K and Peng H 2020 *Nano Lett.* **20** 7469

[28] Kong D, Cha J J, Lai K, Peng H, Analytis J G, Meister S, Chen Y, Zhang H J, Fisher I R, Shen Z X and Cui Y 2011 *ACS Nano* **5** 4698

[29] Irfan B, Sahoo S, Gaur A P S, Ahmadi M, Guinel M J F, Katiyar R S and Chatterjee R 2014 *J. Appl. Phys.* **115** 173506

[30] Zhang J, Peng Z, Soni A, Zhao Y, Xiong Y, Peng B, Wang J, Dresselhaus M S and Xiong Q 2011 *Nano Lett.* **11** 2407

[31] Khan U, Luo Y, Tang L, Teng C, Liu J, Liu B and Cheng H M 2019 *Adv. Funct. Mater.* **29** 1807979

[32] Fu Q, Zhu C, Zhao X, Wang X, Chaturvedi A, Zhu C, Wang X, Zeng Q, Zhou J, Liu F, Tay B K, Zhang H, Pennycook S J and Liu Z 2019 *Adv. Mater.* **31** 1804945

[33] Su G, Hadjiev V G, Loya P E, Zhang J, Lei S, Maharjan S, Dong P M, Ajayan P, Lou J and Peng H 2015 *Nano Lett.* **15** 506

[34] Wu J, Tan C, Tan Z, Liu Y, Yin J, Dang W, Wang M and Peng H 2017 *Nano Lett.* **17** 3021

[35] Tong T, Chen Y, Qin S, Li W, Zhang J, Zhu C, Zhang C, Yuan X, Chen X, Nie Z, Wang X, Hu W, Wang F, Liu W, Wang P, Wang X, Zhang R and Xu Y 2019 *Adv. Funct. Mater.* **29** 1905806